

# A Multi-Robot System for the Study of Face-to-Face Interaction Dynamics

Cinzia Tomaselli , Dario C. Guastella , *Member, IEEE*, Giovanni Muscato , *Senior Member, IEEE*,  
Mattia Frasca , and Lucia Valentina Gambuzza 

**Abstract**—Face-to-face interactions are fundamental to the human social system, and as such, they are a key ingredient in understanding how processes such as opinion dynamics, news and rumor diffusion, and epidemic spreading may occur. In this letter, we leverage the theoretical understanding provided by mathematical models based on complex networks of face-to-face interaction dynamics to propose a multi-robot system that facilitates experimental investigations of these dynamics in settings where the parameters are controllable. Specifically, we consider a team of Elisa-3 robots and implement a distributed and decentralized control law that enables the key mechanisms of interaction giving rise to face-to-face dynamics. We find that the multi-robot system reproduces the main features of the face-to-face dynamics such as long-tailed power-law distributions of contact durations and time intervals between successive contacts. Remarkably, these features prove to be robust, as they emerge in various experimental settings, as well as under challenging operating conditions of the system.

**Index Terms**—Multi-robot systems, agent-based systems, face-to-face interaction dynamics, distributed control.

## I. INTRODUCTION

**S**TUDIES from complexity theory produce elegant mathematical models that are able to explain the underlying mechanisms of many artificial and natural systems where interactions among units are the key ingredient shaping the emerging collective behavior [1], [2], [3]. However, specially when these models are devoted to the analysis of social systems, very often they can be validated against real data, but not compared with the results of controlled experiments. In social systems, in fact, parameters are often given and not controllable. To fill this gap, some works have recently proposed the use of robotic platforms implementing the mathematical model of a complex system and enabling an analog experimentation with tunable parameters [4], [5], [6], [7], [8], [9], [10].

Manuscript received 8 May 2023; accepted 17 August 2023. Date of publication 4 September 2023; date of current version 12 September 2023. This letter was recommended for publication by Associate Editor S. Hauert and Editor M. A. Hsieh upon evaluation of the reviewers' comments. The work of Dario C. Guastella was supported by the Project PON R&I REACT-EU. The work of Mattia Frasca and Giovanni Muscato was supported by the Project Agriculture, Green & Digital (AGREED). This work was supported by the University of Catania, through the PIA.CE.RI. Framework, starting grant for RTDb. (*Corresponding author: Lucia Valentina Gambuzza.*)

The authors are with the Department of Electrical Electronic and Computer Engineering, University of Catania, 95123 Catania, Italy (e-mail: cinzia.tomaselli@phd.unict.it; dario.guastella@unict.it; gmscato@dieei.unict.it; mfrasca@diees.unict.it; lucia.gambuzza@unict.it).

This letter has supplementary downloadable material available at <https://doi.org/10.1109/LRA.2023.3311347>, provided by the authors.

Digital Object Identifier 10.1109/LRA.2023.3311347

A pioneer work in this direction focuses on a special type of consensus dynamics, i.e., the naming game, and implements it on the kilobot robotic platform [4]. The Authors of the study analyze the effects of the physical interference on the concurrent execution of the games, and experimentally demonstrate the emergence of consensus in the naming process. Consensus dynamics has been also used to find the best-of-n solution through voter models using kilobot robots [5], [11]; interestingly, the robots are able to better adapt to environment changes when communication is constrained [5]. Nonequilibrium self-organization phenomena have been also studied with the help of robotic platforms, for instance to test a predictive theory based on rattling [12]. Instead, in [6], [7] a swarm of e-puck robots is used to study the different regimes of synchronization that can appear in a system of mobile pulse-coupled oscillators as a function of agent speed, angle and range of interaction. Real robot experiments have been also used to study the search efficiency and the ability to spread information within a swarm of random walkers [8]. The theoretical model of swarmalators that combines together the synchronization and swarming dynamics has been also implemented in a robotic platform, in particular by using both small robots and drones [9], [10].

These works show how robotics can be useful for the study of complex systems. In fact, it provides a natural embodiment for theoretical models of complex systems [13], [14], and enables the experimental validation of the assumptions on the mechanisms underlying the system dynamical behavior, including the possibility of physical investigations with tunable parameters. However, the cross-fertilization between robotics and complexity [15] can be also beneficial for robotics, as algorithms drawn from the elementary principles of interactions unveiled in complex systems can be particularly useful for the control of multi-agent systems, where typically centralized methods are used instead [16]. An example is the distributed control of agents that sense and react to virtual forces inspired to natural physical laws in a framework enabling self-organization, fault-tolerance, and self-repair [17]. Another example is provided by the distributed control law introduced in [18]. This control law exploits agent elementary interactions and adaptation to design a strategy for geometric pattern formation that avoids the need of communication between agents, relying instead on the calculation of the displacement between the units that can be carried out with low sensor requirements. A third example is the self-organized and decentralized decision-making method that, being able to reach consensus on the fastest

action, allows a swarm of robots to select the shortest of two paths [19].

In this letter, we propose a robotic implementation of the attractiveness-based model for face-to-face interaction networks and study the effect of the physical embodiment on the model dynamics. The attractiveness-based model was introduced in [20] to describe the face-to-face interaction networks that arise in human gatherings. The model is based on simple mechanisms that govern the interactions among the units and enable the formation of dynamic groups, as observed in empirical data sets of human gatherings [21]. These groups play a significant role in social systems as they foster decision-making and problem-solving processes that can leverage the diverse experiences and viewpoints of the individuals within the group to offer more effective solutions and creative decisions [21], [22]. The model shares the advantages with swarm robotics [23] of being a self-organized and distributed approach. Additionally, it offers the further benefit of having an additional parameter, the attractiveness, which can be associated to some feature of the unit that can be leveraged in various potential real-world applications. An example is multi-agent mapping, where the attractiveness could represent a quantity proportional to the area already mapped by each agent. While interacting, the agents can exchange and integrate their maps, thus accelerating the complete reconstruction of the environment. Another application could be related to the energy management of the robot fleet, achieved by assigning an attractiveness value to each agent inversely proportional to its battery level. This, combined with a quick energy transfer solution, could help equalize the battery charge among the robots.

To develop our robotic implementation, we use a team of Elisa-3 robots, that are small autonomous robots equipped with a local communication system and sensors for obstacle avoidance, often used in research applications of swarm robotics, multi-agent systems, and neurorobotics [24], [25], [26], [27], [28], [29], [30]. We find that, under a variety of different experimental conditions, the multi-robot system displays a distribution of the contact duration and of the time interval between consecutive contacts similar to the theoretical model. Interestingly, the same features in the face-to-face interactions also emerge when the multi-robot team is operated in challenging conditions. For instance, this is the case when a very short time is allocated to receive messages from other robots, causing the loss of many interactions that still do not hamper the emergence of the face-to-face dynamics. Altogether these findings demonstrate the robustness of the attractiveness-based algorithm towards physical implementations.

## II. THE ATTRACTIVENESS-BASED MODEL FOR FACE-TO-FACE INTERACTION NETWORKS

The attractiveness-based model for face-to-face interaction networks [20] consists of a group of  $N$  agents distributed on a plane where they move and interact according to the following rules. Each agent is characterized by a parameter  $a_i$ , representing its attractiveness, namely how likely other agents, which get in touch with it, will be engaged in a face-to-face interaction

with it. At each time step  $t_k = k\Delta h$  with  $\Delta h$  constant and  $k = 0, 1, \dots, K$ , an agent can either perform a random walk or remain in its previous position to interact with one or more agents that are attracting its interest. In particular, a stochastic process regulates the action performed by the agent, such that with probability  $p_i(t_k)$  the agent moves and with probability  $1 - p_i(t_k)$  it does not change its position and interacts face-to-face with its neighbors. The probability  $p_i(t_k)$  is a function of the attractiveness of the neighboring agents, namely

$$p_i(t_k) = 1 - \max_{j \in \mathcal{N}_i(t_k)} a_j \quad (1)$$

where  $\mathcal{N}_i(t_k)$  is the neighborhood of agent  $i$  at time  $t_k$ . In more detail, if we indicate with  $\mathbf{x}_i(t_k)$  the position of agent  $i$  in the plane at time  $t_k$  and with  $r$  the sensing radius of each agent, then,  $\mathcal{N}_i(t_k)$  is the set of agents that at time  $t_k$  are at a distance smaller than  $r$ , i.e.,  $\mathcal{N}_i(t_k) = \{j : \|\mathbf{x}_j(t_k) - \mathbf{x}_i(t_k)\|^2 \leq r\}$ .

To introduce the motion equations, let us indicate with  $\mathbf{v}_i(t_k) = \nu e^{i\theta(t_k)}$  the linear velocity of agent  $i$ . Here,  $\nu$  denotes the modulus of the velocity that is maintained constant in time, while  $\theta(t_k)$ , the agent heading, is a quantity that changes randomly at each time step  $\Delta h$ . Then, with probability  $p_i(t_k)$  agent  $i$  performs a random walk and its position is updated as follows

$$\mathbf{x}_i(t_{k+1}) = \mathbf{x}_i(t_k) + \mathbf{v}_i(t_k)\Delta h \quad (2)$$

while with probability  $1 - p_i(t_k)$  its position  $\mathbf{x}_i(t_{k+1})$  remains the same of the previous step, i.e.,  $\mathbf{x}_i(t_{k+1}) = \mathbf{x}_i(t_k)$ .

In view of a robotic implementation of the model there are several aspects to consider. First of all, notice that  $p_i(t_k)$  changes over time, as the neighborhood does. In the original model [20],  $p_i$  is updated with the same step size, namely  $\Delta h$ , of the random walk process. However, in a robotic implementation, where agents are no more dimensionless particles, this strategy is not suitable. On the contrary, obstacle avoidance should always be active in order to avoid collisions with other robots or with the physical boundaries of the arena where they move. In addition, turning/heading update is not instantaneous (as this would imply an infinite angular velocity), but requires a finite time. Finally, the third important ingredient to take into consideration is that the bandwidth of the communication between agents is limited.

To account for these important factors in the physical implementation, here we extend the original attractiveness-based model by revisiting some of the model assumptions and including some further parameters. In the original formulation of the model periodic boundary conditions are considered; here, for the sake of comparison with the experiments, also in the mathematical model we consider that at the boundaries of the arena there are fixed walls. Furthermore, in our numerical simulations, rather than performing the motion step of the random walk in a single time interval, we consider a smaller step size  $\delta h < \Delta h$  and check after each interval of fixed length  $\delta h$  whether during its motion the agent finds an obstacle or not (the obstacle can be one of the arena boundaries or another unit). If there are no encounters, then the full motion step of length  $\nu\Delta h$  is performed, otherwise two situations may occur. If the obstacle is one of the arena walls, the robot stops, rotates to a random direction and, then, continues its random walk. Otherwise, if the obstacle is another unit of the

team, the agent stops at the position of the encounter, effectively performing a random walk step of smaller length. At this point, the agent has to ‘decide’ whether to engage in an interaction or not, according to the probability  $p_i$ . To take into account the limited bandwidth of the communication link between the units, the agent remains at a fixed position for a time interval equal to  $t_s$  and updates its decision at intervals of  $t_s$ . Hence, if an agent decides to engage in an interaction, then the duration of such an interaction will be not shorter than  $t_s$ . Summing up, our model includes two new parameters,  $\delta h$  and  $t_s$ , and the additional rules to account for the obstacle avoidance protocol that needs to be always active in our robotic implementation.

### III. ROBOTIC IMPLEMENTATION

The robotic implementation of the attractiveness-based model for face-to-face interactions has been developed using a team of Elisa-3 robots.<sup>1</sup> These are small-sized robots with a circular shape, diameter  $d = 5$  cm, height  $h = 3$  cm, and weight  $w = 39$  g. Elisa-3 robots are differential drive platforms with two wheels, each driven by a DC motor with a 25:1 reduction gear and maximum speed equal to 60 cm/s.

Each robot has eight IR sensors, uniformly distributed along the external circumference of the chassis and able to detect obstacles at a distance up to 5 cm, and four ground sensors, located on the front-side of the robot and used for cliff avoidance. The IR sensors can also be used for local communication with other robots. As the maximum distance for this communication is  $d_M = 5$  cm, each robot can communicate to any other robot that is at a center-to-center distance between 5 cm and 10 cm. There is no transmission/reception queue in the local communication link and the throughput is about 1 B/s. The local communication system allows the robots to transmit a one-byte packet that we use to send the robot attractiveness.

The experimental setup also includes a 2.4 GHz radio base-station connected to a PC, that can transmit/receive data to/from the robots. In our case, we use it only to collect the information on the robot status needed to reconstruct the time duration of the interactions and the time intervals between two consecutive interactions, respectively indicated as  $\Delta t$  and  $\tau$ . Communication occurs one way, with robots sending the timestamp of the interaction with other units and the PC recording this information for further offline analysis of the system behavior.

Each robot is controlled by an onboard 8-bit Atmel ATmega2460 microcontroller that handles motor control, sensor data acquisition and communication with other robots and the PC. Robots move in an arena of dimensions  $L_x$  and  $L_y$  as schematically represented in Fig. 1, which also illustrates the radius of local communication,  $r$ . This is an important parameter for the dynamics as interactions can occur only with robots within this radius. On top of the arena, an RGB camera allowing to record the robot trajectories is mounted.

The control of the robot autonomous behavior is carried out through a finite state machine that implements the mechanisms of interaction and movement of the attractiveness-based model

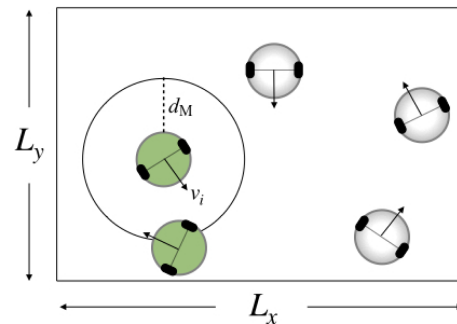


Fig. 1. Schematic representation of the team of Elisa-3 robots implementing attractiveness-based face-to-face dynamics. Robots represented in green color are communicating to each other through the local communication system (with  $d_M$  indicating the maximum distance for such a communication), while the other units (in gray color) are not detecting other robots or obstacles within their communication/sensing radius and, hence, are moving as random walkers.

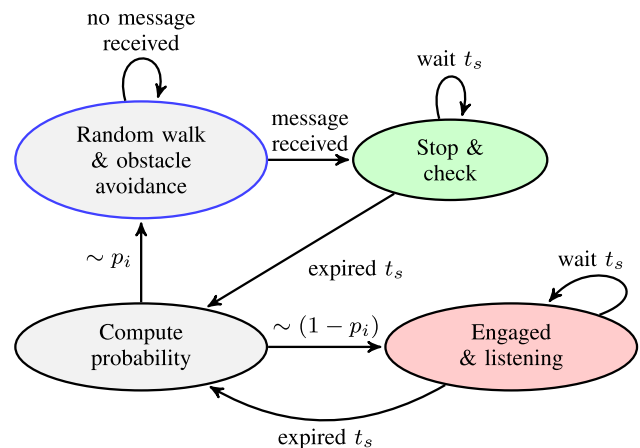


Fig. 2. Finite state machine used to control the autonomous behavior of each robot of the team. The finite state machine is initialized in the ‘Random walk & obstacle avoidance’ state (visually highlighted in the scheme with a blue contour).

for face-to-face dynamics. As shown in Fig. 2, the state machine has four states: ‘Random walk & obstacle avoidance’, ‘Stop & check’, ‘Compute probability’, and ‘Engaged & listening’. In the first state, the robot moves as a random walker along the arena, while avoiding potential obstacles and continuously checking whether a message from other robots is received. When this occurs, the state machine moves to the ‘Stop & check’ state, where the robot stops at the current position for a period of time equal to  $t_s$ , searching for eventual messages from other robots and retrieving the value of the attractiveness of the neighboring robots. After that, it moves to the ‘Compute probability’ state where the robot calculates  $p_i$  according to (1). At this point, with probability  $1 - p_i$  moves to the ‘Engaged & listening’ state, thus starting a face-to-face interaction, or with probability  $p_i$  goes back to the ‘Random walk & obstacle avoidance’ state, thus moving away from the current position as the other robots (if any) have not raised its interest. The ‘Engaged & listening’ state, therefore, represents the condition where the robot is effectively interacting face-to-face with other robots, forming a group of two or more units. From this state, where messages from other

<sup>1</sup>[Online]. Available: <https://www.gctronic.com/doc/index.php/Elisa-3>

**Algorithm 1:** Face-to-Face Dynamics for Agent  $i$ .

---

```

Parameter      :  $a_i, t_s, t_f, \nu$ 
Initialization : State = RandomWalk
1 while true do
2   Broadcast  $a_i$ 
3   Check IR sensors
4   if ( $messageReceived==true$ ) then
5     Stop moving
6     State = MsgReceived
7   end
8   switch State do
9     case RandomWalk do
10      Move as a random walker with obstacle avoidance
11    end
12  end
13  case MsgReceived do
14    Turn on green light
15    Wait  $t_s$ 
16    State = ComputeProb
17  end
18  case ComputeProb do
19    Compute  $p_i$  as in Eq. (1)
20    Generate a random number  $\xi \in [0, 1]$ 
21    if  $\xi < p_i$  then
22      State = RandomWalk
23    else
24      State = Engaged
25    end
26  end
27  case Engaged do
28    Turn on red light
29    Wait  $t_s$ 
30    State = ComputeProb
31  end
32 end

```

---

robots are also continuously checked, after a period of time equal to  $t_s$ , the robot moves back to ‘Compute probability’ from which the robot decides to continue the face-to-face interaction (with probability  $1 - p_i$ ) or leave the group (with probability  $p_i$ ). In the two states ‘Stop & check’ and ‘Engaged & listening’ the robot’s LED turns green and red respectively, in order to help to visually detect in which state the robot is. The finite state machine is implemented in the robot via Algorithm 1.

When the robot is not interacting with other units, it moves as a random walker with obstacle avoidance control always active. Taking into account that the robots are controlled by differential drive, we implemented the random walk in two steps. In the first step, we randomly set the direction of rotation of the robot (left or right) and then rotate it for a time equal to  $t_R$  which is randomly drawn with uniform distribution in the interval  $[0.1 s, 1s]$ . This results in an in-place rotation of the robot by an angle randomly drawn with uniform distribution in the interval  $[-\pi, \pi]$ . Then, in the second step, the robot moves forward for a period of time equal to  $t_f$  (which corresponds to  $\Delta h$  in (2)) with fixed velocity  $\nu$ . Notice that, since obstacle avoidance is always active,  $\nu t_f$  represents the maximum distance of the random walk step, while it is the exact distance only when no obstacles (either the arena walls or other robots) are encountered during this motion step. Obstacle avoidance is implemented by continuously checking eventual obstacles via the IR sensors. When the sensors signal the presence of an obstacle, then either this obstacle is a robot (as simultaneously a message has been received) and the finite state machine moves to the ‘Stop & check’ state, or it is a wall

TABLE I  
LIST OF SYMBOLS

Symbol	Parameter
$t_s$	time for local communication
$t_R$	rotation time
$t_f$	forward time
$\nu$	robot velocity
$a_i$	attractiveness of robot $i$
$L_x, L_y$	length and width of the arena
$\rho$	robot density
$T_M$	test duration

of the arena. In this latter case, the robot heading is randomly changed in the  $[-\pi, \pi]$  interval and, then, the robot continues its motion step.

An important parameter of our experiments is the time that a robot has to wait to correctly receive a message after the IR sensors have detected it. This parameter is briefly indicated as the time for local communication  $t_s$ . The nominal value of the local communication throughput for the Elisa-3 robot is about 1 B/s; however, based on a series of preliminary experiments that we have run to investigate whether the value of  $t_s$  could be reduced, we have selected  $t_s = 700$  ms as a trade-off between message loss and the time the robot has to spend while waiting for messages.

During the experiments, the robots also communicate their status, including potential interactions with other units, to a PC through the radio link, at time intervals of 100 ms. Communication with the PC is solely used to record the relevant information to analyse the collective behavior of the system, but not for the robot control law which is fully decentralized and distributed.

Two other important parameters of the setup are  $\nu$  and  $t_f$ , that we have been empirically set to 6 cm/s and 2 s, respectively. These are trade-off values between the size of the area explored by a robot during its motion (which becomes larger as the two parameters increase) and the probability of receiving messages from other robots (which decreases as the two parameters increase).

Finally, two other parameters influence the collective behavior of the whole system of interacting robots. They are the robot density  $\rho$  and the values of the attractiveness of each robot, stored in a single vector  $\mathbf{a} = [a_1, a_2, \dots, a_6]^T$ . As the number of robots is kept fixed, the density of the robots is determined by the dimensions of the arena, namely  $\rho = N/(L_x L_y)$ . The values of attractiveness are set in the interval  $[0, 1]$  and are assigned to each robot of the team at the beginning of each trial and then kept constant. The main symbols used in the letter are summarized in Table I.

#### IV. EXPERIMENTAL RESULTS

To illustrate our results, we first discuss an experiment for a fixed setting of the system parameters. In particular, here we have considered  $N = 6$  robots moving in an arena with  $L_x = 80$  cm and  $L_y = 60$  cm, thus resulting in a density of robots equal to  $\rho = 1.3 \times 10^{-3}$ .<sup>2</sup> The robot attractiveness is fixed as:  $\mathbf{a} = [0.75, 0.88, 0.93, 0.67, 0.72, 0.67]$ . Fig. 3 shows five snapshots

<sup>2</sup>The density is always expressed in robots/cm<sup>2</sup>

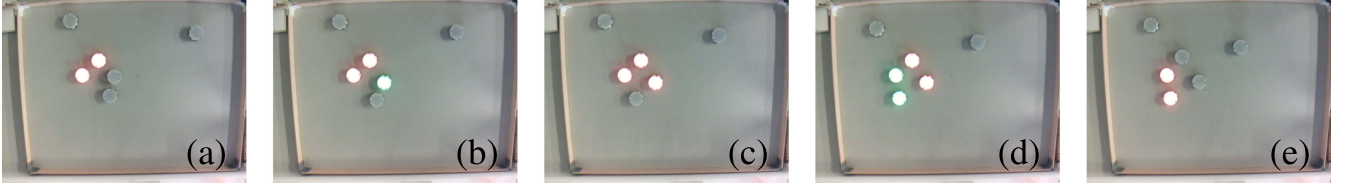


Fig. 3. Dynamical evolution of group formation in an experiment made with  $N = 6$  Elisa-3 robots. The different snapshots are taken from the supplementary video (available at <https://ieeexplore.ieee.org>) at the following times: (a)  $t = 63$  s, (b)  $t = 64$  s, (c)  $t = 65$  s, (d)  $t = 66$  s, and (e)  $t = 67$  s. The units lighting up with red (green) light are interacting (communicating) each other, while no light indicates that the robot is performing a random walk. (a) The robots form a group of two units that are engaged into a face-to-face interaction. (b) A third robot is communicating with one of the two units of the group. (c) The group is now formed by three interacting units. (d) Another robot in the area is communicating with units in the group. (e) The previous group breaks apart and a new group of two units forms, while the other two robots, belonging to the previous group, move away from the area of the meeting.

of a video recording available as supplemental material. It shows the dynamical evolution of the formation of groups in the system. Initially, two robots form a group (Fig. 3(a)). Later, another robot communicates with one of the group units and joins it (Fig. 3(b) and (c)). Subsequently, a different unit communicates with a member of the group (Fig. 3(d)), and engages in a face-to-face interaction to form a new group of two robots (Fig. 3(e)), while the previous group breaks apart.

We have then conducted a more systematic investigation by exploring various parameter settings and performing a statistical analysis of the data gathered during our experiments to determine the distribution of the contact duration, denoted as  $P(\Delta t)$ , as well as the distribution of the time interval, denoted as  $P(\tau)$ , between two consecutive interactions of a robot with some other unit. Here, with the term contact we indicate the engagement in a face-to-face interaction of two or more robots. In particular, we have considered exemplificative settings with different values of the density  $\rho$  and the attractiveness vector  $\mathbf{a}$ . To change  $\rho$ , we have kept fixed the number of robots and changed the size of the arena (in particular, varying  $L_x$ ), whereas the attractiveness vector  $\mathbf{a}$  has been set via robot programming. The time for local communication between the robots has been set to  $t_s = 700$  ms in all the experiments where not differently mentioned. The same holds for the speed module that is fixed to  $\nu = 6$  cm/s.

We first discuss the effect of the density, considering two different values of  $\rho$ , namely  $\rho_1 = 1.3 \times 10^{-3}$ , obtained by setting  $L_x = 80$  cm and  $L_y = 60$  cm, and  $\rho_2 = 2.5 \times 10^{-3}$ , obtained by resizing the arena such that  $L_x = 40$  cm and  $L_y = 60$  cm. The results are illustrated in Fig. 4 that shows the distribution of the contact duration,  $P(\Delta t)$ , and that of the time intervals,  $P(\tau)$ , for  $\rho = \rho_1$  (blue circles), and  $\rho = \rho_2$  (orange squares). Both distributions are obtained by dividing the empirical data into bins and reporting the number of observations for each bin divided by the total number of observations. The results are averaged over 10 different runs, in each of which the behavior of the robots was monitored for a period of time equal to  $T_M = 10$  min. The robot attractiveness is fixed to  $\mathbf{a} = [0.75, 0.88, 0.93, 0.67, 0.72, 0.67]$ , such that the average value is equal to  $\langle a_i \rangle = 0.77$ .

We notice that, for both values of  $\rho$ , the two distributions  $P(\Delta t)$  and  $P(\tau)$  display a long-tailed power-law form spanning few orders of magnitude. This is in agreement with the analysis of the original mathematical model where this behavior is consistently observed for different settings of the parameters [20]. From the analysis of  $P(\Delta t)$  (Fig. 4(a)), we find that the number

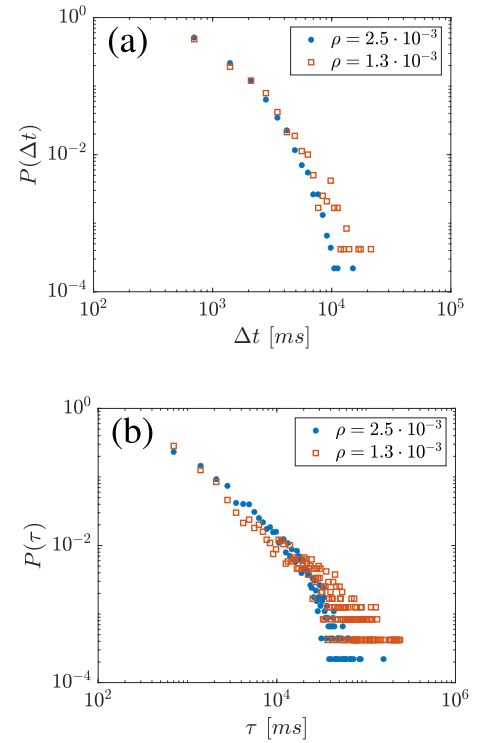


Fig. 4. Experimental results. Effect of the density on the distribution of the contact duration,  $P(\Delta t)$ , (a) and on the distribution of the time interval between consecutive contacts,  $P(\tau)$ , (b). The results are the average of 10 runs for each density value, that is controlled by changing  $L_x$  ( $L_x = 80$  cm for the first set of runs, represented with blue circles,  $L_x = 40$  cm for the second one, represented with orange squares). The remaining parameters are fixed to:  $t_s = 700$  ms,  $L_y = 60$  cm,  $T_M = 10$  min,  $t_f = 2$  s,  $\nu = 6$  cm/s,  $t_r \in [100 \text{ ms}, 1 \text{ s}]$ ,  $N = 6$ , and  $\langle a_i \rangle = 0.77$ .

of contacts with small duration is high, whereas there are few cases where the duration of the contact between robots is large. Analogously, the behavior of  $P(\tau)$  (Fig. 4(b)) is also characterized by a long-tailed power-law distribution, meaning that there are few contacts occurring after long time intervals and many after small time intervals. The density  $\rho$  seems to significantly affect the distribution of  $\tau$  (Fig. 4(b)), where we notice that, for the larger value of density, it is more difficult to observe larger time intervals compared to the case of smaller density. Instead, the density has a smaller effect on the distribution of contact duration, with the more noticeable impact on the tail of the distribution.

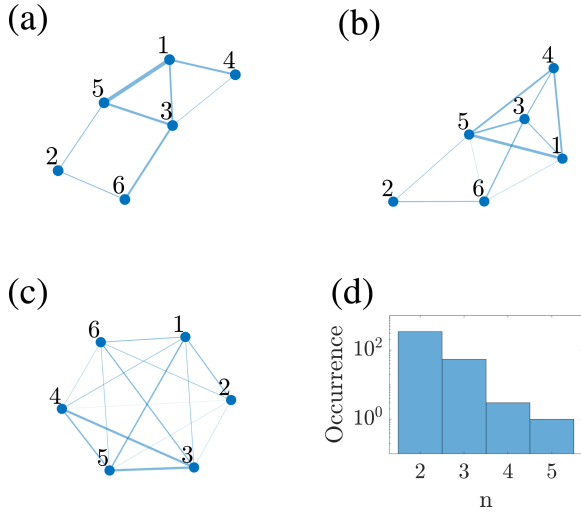


Fig. 5. Interactions among agents and group formation in an experiment with  $N = 6$  Elisa-3 robots. Aggregated network illustrating the number of interactions among agents after 1 minute (a), 3 minutes (b), and 10 minutes (c), and occurrences of groups of size  $n$  during robot experiment (d). The experiment has been carried out using the following parameters:  $t_s = 700$  ms,  $L_x = 40$  cm,  $L_y = 60$  cm,  $T_M = 10$  min,  $t_f = 2$  s,  $\nu = 6$  cm/s,  $t_r \in [100$  ms, 1 s], and  $\langle a_i \rangle = 0.77$ .

During their motion, robots interact with other robots in a dynamical way, forming groups of different size. This can be illustrated by considering the number of interactions between each pair of robots and counting the occurrence of the group size during a robot experiment. Fig. 5(a)–(c) reports the aggregated network obtained by considering all interactions taking place between pairs of robots in time windows of increasing duration. The aggregated network is represented with edges of thickness proportional to the amount of interactions, normalized with respect to the total number of interactions in that time window. For a time window of small duration, not all pairs of nodes are connected, as during their motion the robots did not have the chance to meet all the other units. As more time elapses, more links emerge, up to the point where the aggregated network is a complete graph, with the weights reflecting the stochasticity in the robot dynamics. Fig. 5(d) reports the occurrence of groups of different size  $n$ . As expected, smaller groups occur more frequently than larger ones.

Next, we discuss the experiments we have carried out to investigate the effects of different values of the robot attractiveness. In particular, we have considered two sets of values for  $\mathbf{a}$ :  $\mathbf{a} = \mathbf{a}_1 = [0.75, 0.88, 0.93, 0.67, 0.72, 0.67]$ , representing a scenario where the average attractiveness is high, i.e.,  $\langle a_i \rangle = 0.77$ , and  $\mathbf{a} = \mathbf{a}_2 = [0.40, 0.76, 0.62, 0.55, 0.42, 0.67]$ , representing a scenario with a lower value of average attractiveness, i.e.,  $\langle a_i \rangle = 0.57$ . The distributions  $P(\Delta t)$  and  $P(\tau)$  obtained under these conditions are reported in Fig. 6. Here, we have considered  $\rho = 2.5 \times 10^{-3}$ , while the other parameters, such as the number of agents  $N$ , the robot velocity  $\nu$ , the experiment duration  $T_M$ , and the time for local communication  $t_s$  are fixed as in the previous set of experiments. Also in this case, we find that, for all values of  $\mathbf{a}$ , both  $P(\Delta t)$  and  $P(\tau)$  follow a long-tailed power law. Here, we notice that, while

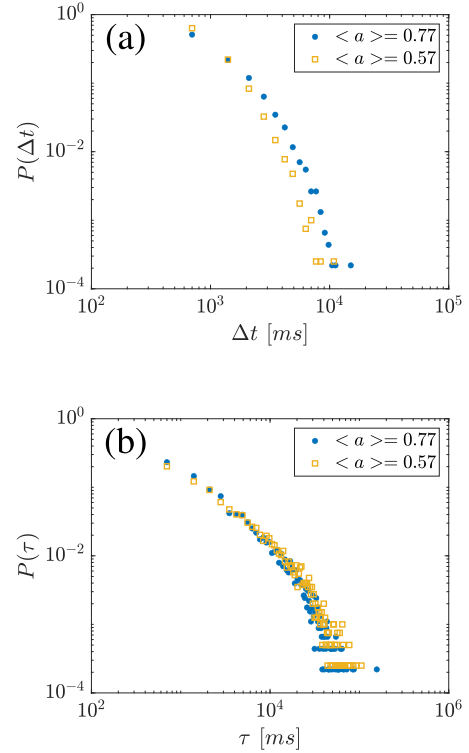


Fig. 6. Experimental results. Effects of the robot attractiveness,  $\mathbf{a}$ , on the distribution of the contact duration,  $P(\Delta t)$ , (a) and on the distribution of the time interval between consecutive contacts,  $P(\tau)$ , (b). The results are the average of 10 runs for each value of  $\mathbf{a}$  (in the first case, represented with blue circles, the robot attractiveness is such that  $\langle a_i \rangle = 0.77$ , while in the second case, represented with yellow squares, is such that  $\langle a_i \rangle = 0.57$ ). The remaining parameters are fixed to:  $t_s = 700$  ms,  $L_x = 40$  cm,  $L_y = 60$  cm,  $T_M = 10$  min,  $t_f = 2$  s,  $\nu = 6$  cm/s,  $t_r \in [100$  ms, 1 s], and  $N = 6$ .

changing the attractiveness has a low impact on  $P(\tau)$  (Fig. 6(b)), it significantly affects the distribution of the contact duration  $P(\Delta t)$  (Fig. 6(a)). When the average value of attractiveness is lower, the number of contacts with short duration increases, while the number of contacts with long duration decreases, compared to the case where the attractiveness values are higher.

The face-to-face dynamics experimentally obtained has been then compared with numerical simulations of the model discussed in Section II. We have found that the model can produce contact durations and time intervals between consecutive contacts having distributions similar to those observed experimentally, when faults in the local communication among agents are explicitly taken into account in the model. To this aim, we have introduced in the model a further parameter,  $p$ , mimicking the effect of loss of messages. This parameter represents the probability that each neighboring agent of a generic unit  $i$  is correctly perceived as such and, therefore, able to exchange information with it. Hence, with probability  $1 - p$ , agent  $i$  misses the message sent by the other agent, despite it is one of its neighbors, and, thus, does not take into account its attractiveness in evaluating (1). In the robotic experiments, the loss of messages depends on the time for local communication,  $t_s$ , on the robot motion and on the asynchronous communication, and, as such, it is difficult to estimate. For this reason, in our

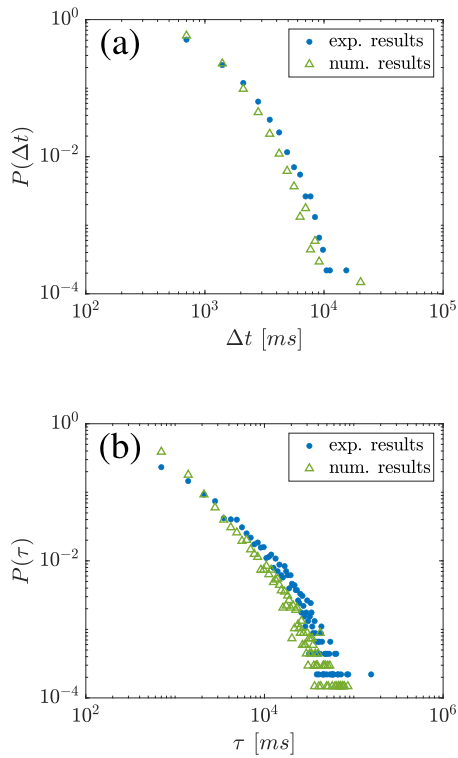


Fig. 7. Comparison of experimental and numerical results. Distribution of the contact duration,  $P(\Delta t)$ , (a) and distribution of the time interval between consecutive contacts,  $P(\tau)$ , (b) of experimental and numerical data with  $p = 0.1$ . The results are the average of 10 runs for each type of test, the experimental data are represented by blue circles, while the numerical ones are represented by green triangles. The system parameters are fixed as:  $t_s = 700$  ms,  $L_x = 40$  cm,  $L_y = 60$  cm,  $T_M = 10$  min,  $t_f = 2$  s,  $\nu = 6$  cm/s,  $N = 6$ , and  $\langle a_i \rangle = 0.77$ . For numerical simulations, we used  $\Delta h = 2$  s,  $\delta h = 100$  ms, and  $K = 300$ , which corresponds to  $T_M = K\Delta h = 10$  min.

analysis the parameter  $p$  has been empirically set to the value  $p = 0.1$ .

We illustrate the comparison between experiments and simulations with reference to the case  $\rho = \rho_2$  and  $\mathbf{a} = \mathbf{a}_1$ , noting that similar results have been obtained for other settings of the parameters. The distributions  $P(\Delta t)$  and  $P(\tau)$ , obtained experimentally and numerically for these values of the parameters, are shown in Fig. 7. Although the distributions are similar, there are still some differences. In particular, in the experimental case we find slightly longer time intervals between consecutive contacts. This suggests that other quantities, not explicitly taken into account in the model (such as the finite time for heading change or robot deviations from straight motion), are also influencing the behavior of the multi-robot system.

Finally, we discuss an example where robots are operated under challenging conditions. Specifically, we set  $t_s = 500$  ms, which allocates a very short time window for message reception in the local communication system. This time window is below the inverse of the nominal throughput, resulting in a large loss of messages. Despite this, the main features of face-to-face interaction dynamics still emerge. As shown in Fig. 7(a), the distribution of contact durations is characterized by only a few points, as long-duration contacts become unlikely. However, these points

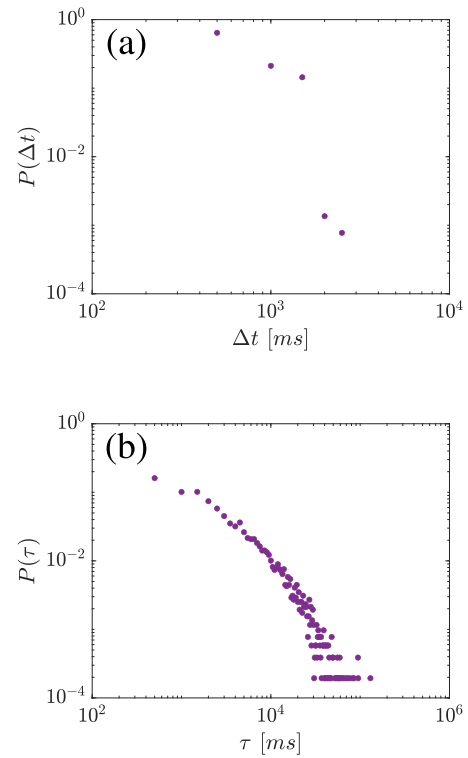


Fig. 8. Experimental results. Distribution of the contact duration,  $P(\Delta t)$ , (a) and distribution of the time interval between consecutive contacts,  $P(\tau)$ , (b). The results are the average of 10 runs with the following parameters:  $t_s = 500$  ms,  $L_x = 40$  cm,  $L_y = 60$  cm,  $\delta t = 100$  ms,  $T_M = 10$  min,  $t_f = 2$  s,  $\nu = 6$  cm/s,  $t_r \in [100$  ms, 1 s],  $N = 6$ , and  $\langle a_i \rangle = 0.77$ .

still distribute according to a power law. On the other hand, as shown in Fig. 7(b), the adverse operating conditions considered in this experiment do not seem to impact the distribution of time intervals between successive contacts, which contains many points and displays a long-tailed power-law form similar to those observed for other settings of the system parameters.

## V. CONCLUSION

In this work, we have introduced a robotic implementation of the attractiveness-based model for face-to-face interaction dynamics. The model considers elementary mechanisms of interactions that are locally implemented in each robot in a fully distributed and decentralized manner. This is an interesting feature of the control law, that could pave the way to real-world applications, where obtaining a dynamical group formation is relevant. On the other hand, the proposed system serves as a platform for the experimental investigation of face-to-face dynamics in an environment with tunable parameters, and is of interest for studies in complexity theory. Our results demonstrate the robustness of the approach against many factors present in a real environment that are usually neglected in numerical simulations, such as communication noise, presence of faults, non-idealities in robot motion, and so on. In this perspective, the result on effect of the limited bandwidth of inter-robot communication is particularly relevant, as the main features of face-to-face dynamics also emerge when the local communication system

is operated under challenging conditions. Future work may be directed towards the study of the behavior of the multi-agent system in presence of directional sensors and communication, or multiple sensing and communication systems to exploit under varying environment conditions. The multi-robot system also prompts further experimental studies of interesting aspects of face-to-face dynamics in social systems, such as the effect of attractiveness values associated with pairs of agents, rather than being a property of the agent itself, or the impact of multiple values of attractiveness coding for different properties of the agent. Another possibility to consider is that the attractiveness changes in time. This could either model agent popularity that is reinforced as more interactions occur, or be function of some features of the agent or the environment it senses.

#### REFERENCES

- [1] S. Thurner, R. Hanel, and P. Klimek, *Introduction to the Theory of Complex Systems*. Oxford, U.K.: Oxford Univ. Press, 2018.
- [2] S. Boccaletti, V. Latora, Y. Moreno, M. Chavez, and D.-U. Hwang, "Complex networks: Structure and dynamics," *Phys. Rep.*, vol. 424, no. 4/5, pp. 175–308, 2006.
- [3] V. Latora, V. Nicosia, and G. Russo, *Complex Networks: Principles, Methods and Applications*. Cambridge, U.K.: Cambridge Univ. Press, 2017.
- [4] V. Trianni, D. De Simone, A. Reina, and A. Baronchelli, "Emergence of consensus in a multi-robot network: From abstract models to empirical validation," *IEEE Robot. Automat. Lett.*, vol. 1, no. 1, pp. 348–353, Jan. 2016.
- [5] M. S. Talamali, A. Saha, J. A. Marshall, and A. Reina, "When less is more: Robot swarms adapt better to changes with constrained communication," *Sci. Robot.*, vol. 6, no. 56, 2021, Art. no. eabf1416.
- [6] F. Perez-Diaz, R. Zillmer, and R. Groß, "Firefly-inspired synchronization in swarms of mobile agents," in *Proc. 14th Int. Conf. Auton. Agents Multiagent Syst.*, 2015, pp. 279–286.
- [7] F. Perez-Diaz, S. M. Trenkwalder, R. Zillmer, and R. Groß, "Emergence and inhibition of synchronization in robot swarms," in *Proc. Distrib. Autono. Robot. Syst.* 2018, pp. 475–486.
- [8] C. Dimidov, G. Oriolo, and V. Trianni, "Random walks in swarm robotics: An experiment with kilobots," in *Proc. Int. Conf. Swarm Intell.*, 2016, pp. 185–196.
- [9] A. Barciś, M. Barciś, and C. Bettstetter, "Robots that sync and swarm: A proof of concept in ROS 2," in *Proc. IEEE Int. Symp. Multi-Robot Multi-Agent Syst.*, 2019, pp. 98–104.
- [10] A. Barciś and C. Bettstetter, "Sandsbots: Robots that sync and swarm," *IEEE Access*, vol. 8, pp. 218752–218764, 2020.
- [11] M. Crosscombe, J. Lawry, S. Hauert, and M. Homer, "Robust distributed decision-making in robot swarms: Exploiting a third truth state," in *Proc. IEEE/RSJ Int. Conf. Intell. Robots Syst.*, 2017, pp. 4326–4332.
- [12] P. Chvykov et al., "Low rattling: A predictive principle for self-organization in active collectives," *Science*, vol. 371, no. 6524, pp. 90–95, 2021.
- [13] M. Frasca, A. Buscarino, A. Rizzo, L. Fortuna, and S. Boccaletti, "Synchronization of moving chaotic agents," *Phys. Rev. Lett.*, vol. 100, no. 4, 2008, Art. no. 44102.
- [14] M. Starnini, M. Frasca, and A. Baronchelli, "Emergence of metapopulations and echo chambers in mobile agents," *Sci. Rep.*, vol. 6, no. 1, pp. 1–8, 2016.
- [15] M. Alhafnawi, E. R. Hunt, S. Lemaignan, P. O'Dowd, and S. Hauert, "Deliberative democracy with robot swarms," in *Proc. IEEE/RSJ Int. Conf. Intell. Robots Syst.*, 2022, pp. 7296–7303.
- [16] D. C. Guastella, L. Cantelli, G. Giannello, C. D. Melita, G. Spatino, and G. Muscato, "Complete coverage path planning for aerial vehicle flocks deployed in outdoor environments," *Comput. Elect. Eng.*, vol. 75, pp. 189–201, 2019.
- [17] W. M. Spears, D. F. Spears, J. C. Hamann, and R. Heil, "Distributed, physics-based control of swarms of vehicles," *Auton. Robots*, vol. 17, no. 2/3, pp. 137–162, 2004.
- [18] A. Giusti, G. C. Maffettone, D. Fiore, M. Coraggio, and M. di Bernardo, "Distributed control for geometric pattern formation of large-scale multi-robot systems," 2022, *arXiv:2207.14567*.
- [19] A. Scheidler, A. Brutschy, E. Ferrante, and M. Dorigo, "The  $k$ -unanimity rule for self-organized decision-making in swarms of robots," *IEEE Trans. Cybern.*, vol. 46, no. 5, pp. 1175–1188, May 2016.
- [20] M. Starnini, A. Baronchelli, and R. Pastor-Satorras, "Modeling human dynamics of face-to-face interaction networks," *Phys. Rev. Lett.*, vol. 110, no. 16, 2013, Art. no. 168701.
- [21] M. Starnini, A. Baronchelli, and R. Pastor-Satorras, "Model reproduces individual, group and collective dynamics of human contact networks," *Social Netw.*, vol. 47, pp. 130–137, 2016.
- [22] M. Buchanan, *The Social Atom: Why the Rich Get Richer, Cheaters Get Caught, and Your Neighbor Usually Looks Like You*. London, U.K.: Bloomsbury Publishing USA, 2008.
- [23] M. Brambilla, E. Ferrante, M. Birattari, and M. Dorigo, "Swarm robotics: A review from the swarm engineering perspective," *Swarm Intell.*, vol. 7, pp. 1–41, 2013.
- [24] M. Schranz, M. Umlauf, M. Sende, and W. Elmenreich, "Swarm robotic behaviors and current applications," *Front. Robot. AI*, vol. 7, pp. 1–20, 2020.
- [25] N. Maruyama et al., "Designing a robotic platform controlled by cultured neural cells," in *Proc. ALIFE 14: The 14th Int. Conf. Synth. Simul. Living Syst.*, 2014, pp. 769–770.
- [26] S. Adams, D. J. Ornia, and M. Mazo, "A self-guided approach for navigation in a minimalistic foraging robotic swarm," *Auton. Robots*, pp. 1–16, 2023.
- [27] G. Franzè, G. Fedele, A. Bono, and L. D'Alfonso, "Reference tracking for multiagent systems using model predictive control," *IEEE Trans. Control Syst. Technol.*, vol. 31, no. 4, pp. 1884–1891, Jul. 2023.
- [28] A. Bono, G. Fedele, and G. Franzè, "A swarm-based distributed model predictive control scheme for autonomous vehicle formations in uncertain environments," *IEEE Trans. Cybern.*, vol. 52, no. 9, pp. 8876–8886, Sep. 2022.
- [29] G. Fedele, L. D'Alfonso, and A. Bono, "Swarm fixed-time reference tracking: A discrete model," *Int. J. Control*, vol. 96, no. 1, pp. 238–250, 2023.
- [30] M. Lewis, L. Canamero, and N. Fineberg, "A robot model of oc-spectrum disorders: Design framework, implementation and first experiments," *Comput. Psychiatry*, vol. 3, pp. 40–75, 2019.